Electromagnetic Imaging for Shape and Variable Conductivity

Wei Chien, Chien-Ching Chiu

Electrical Engineering Department, Tamkang University, Tamsui, Taiwan, Republic of China

ABSTRACT: We consider the inverse problem of determining both the shape and the conductivity of a two-dimensional (2D) conducting scatterer from the knowledge of the far-field pattern of TM waves by solving the ill-posed nonlinear equation. Based on the boundary condition and measured scattered field, a set of nonlinear integral equations is derived and the imaging problem is reformulated into an optimization problem. Satisfactory reconstructions are achieved by the genetic algorithm. Numerical results demonstrate that, even when the initial guess is far away from the exact one, good reconstruction can be obtained. In addition, the effect of Gaussian noise on the reconstruction results is investigated. The numerical results show that multiple incident directions permit good reconstruction of shape and, to a lesser extent, conductivity in the presence of noise in measured data. © 2004 Wiley Periodicals, Inc. Int J RF and Microwave CAE 14: 433–440, 2004.

Keywords: variable conductivity; genetic algorithm; inverse scattering

I. INTRODUCTION

This article deals with the question of determining both the shape and the variable conductivity from the knowledge of the far-field pattern of a scattered wave for a set of incident TM waves.

The usual inverse-obstacle scattering problem is to determine the shape of the obstacle, given information about the far-field pattern of the scattered wave from each of a set of incident fields. In addition, we try to recover the shape of the obstacle, given that it has variable conductivity. Carrying this idea further, we can ask if it is possible, by modifying the conductivity values of the boundary of an obstacle, to make it appear (from a scattering experiment standpoint) as some object of a different shape.

In the past 20 years, many rigorous methods have been developed to solve the exact equation. However,

the inverse problem of this type is difficult to solve because it is ill-posed and nonlinear [1]. As a result, many inverse problems are reformulated as optimization problems. Generally speaking, two main kinds of approaches have been developed. The first is based on gradient-search approach, such as the Newton–Kantorovitch method [2–4], the Levenberg–Marguart algorithm [6–8], and the successive-overrelaxation method [9]. These approaches apply the gradient-search method to find the extreme of the cost function. This method is highly dependent upon the initial guess and tends to get trapped in a local extreme. In contrast, the second approach is based on the genetic algorithm [10–12]. The genetic algorithm is a well-known algorithm that uses stochastic random choice to search through the coding of a parameter space. Compared to gradient search-optimization techniques, the genetic algorithm is less prone to convergence to a local minimum, which in turn renders it an ideal candidate for global optimization. It usually converges to the global extreme of the problem, no matter what the initial estimate is [13]. However, the afore-

mentioned genetic algorithm merely deals with the case of perfectly conducting objects, and there is still no research for the case involving variable conducting metallic scatterers.

In this article, the electromagnetic imaging of a variable conducting cylinder in free space is investigated. The genetic algorithm is used to recover not only the shape, but also the conductivity of a scatterer, by using only the scattered field. The method is potentially important in medical imaging and biological application. In section II, a theoretical formulation for the electromagnetic imaging is presented. The general principle of genetic algorithms and the way we apply them to the imaging problem are described. The numerical results for objects of different shapes and conductivities are given in section III. Finally, some conclusions are drawn in section IV.

II. THEORETICAL FORMULATION

Let us consider a variable conducting cylinder with conductivity $\sigma(\theta)$ located in free space and let ε_0 and μ_0 denote the permittivity and permeability of free space, respectively. The metallic cylinder's cross section, which is described in polar coordinates in the x–y plane by the equation $\rho = F(\theta)$ (that is, the object has a starlike shape), is illuminated by an incident plane wave whose electric-field vector is parallel to the Z axis, that is, transverse magnetic (TM) polarization. We assume that the time dependence of the field is harmonic with the factor $\exp(j\omega t)$. Let $\vec{E}_i$ denote the incident field with incident angle ϕ, as shown in Figure 1. Then, the incident field is given by

$$\vec{E}_i(x, y) = e^{-jk(x \sin \phi + y \cos \phi)}\hat{z}, \quad k^2 = \omega^2 \varepsilon_0 \mu_0. \quad (1)$$

At an arbitrary point (x, y) in Cartesian coordinates or (r, θ) in polar coordinates outside the scattered field, $\vec{E}_s = \vec{E} - \vec{E}_i$ can be expressed by

$$E_s(x, y) = -\int_0^{2\pi} \frac{j}{4} H_0^{(2)}$$

$$\cdot (k\sqrt{(x - F(\theta')\cos(\theta'))^2 + (y - F(\theta')\sin(\theta'))^2})J(\theta')d\theta'$$

$$(2)$$

with

$$J(\theta) = -j\omega\mu_0 \sqrt{F^2(\theta) + F'^2(\theta)}\, J_s(\theta),$$
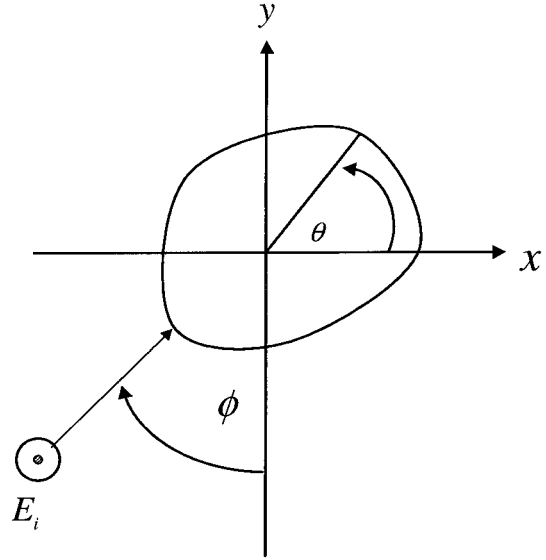
Figure 1. Geometry of the problem in the *x*–*y* plane.

where $H_0^{(2)}$ is the Hankel function of the 2nd order zero, and $J_s(\theta)$ is the induced surface-current density, which is proportional to the normal derivative of the electric field on the conductor surface. Note that the scattered field for large values of r in eq. (2) can be expressed in asymptotic form as

$$E_s(x, y) \approx \frac{e^{-jkr}}{\sqrt{r}}\, G_s(\theta),$$

$$G_s(\theta) = -\frac{j}{4}\sqrt{\frac{2}{\pi k}}\, e^{j\pi/4} \int_0^{2\pi} e^{jkF(\theta')\cos(\theta - \theta')}J(\theta')d\theta',$$

$$(2a)$$

where $G_s(\theta)$ is the scattered far-field pattern. For an imperfectly conducting scatterer with finite conductivity, the electromagnetic wave is able to penetrate into the interior of a scatterer, so that the total tangential electric field at the surface of the scatterer is not equal to zero. As described in [13, 14], the boundary condition for this case can be approximated by assuming that the total tangential electric field on the scatterer surface is related to surface-current density through a surface impedance $Z_s(\omega)$ as follows:

$$\hat{n} \times \vec{E} = \hat{n} \times (Z_s\vec{J}_s), \quad (3)$$

where $\hat{n}$ is the outward unit vector normal to the surface of the scatterer. The scatterer of interest here is a nonmagnetic ($\mu = \mu_0$), variable conducting cylinder with minimum radius of curvature a. The sur-

face impedance is expressed in [14, 15] as $Z_s(\omega, \theta) \cong \sqrt{J\omega\mu_0/\sigma(\theta)}$. This approximation is valid as long as $|\text{Im}(N_c)ka| \gg 1$ and $\sigma \gg \omega\varepsilon_0$, where Im denotes taking the imaginary part, and N_c is the complex index of refraction of the conductor, given by $N_c = \sqrt{1 + [\sigma(\theta)/j\omega\varepsilon_0]}$. The boundary condition at the surface of the scatterer given by eq. (3) then yields an integral equation for $J(\theta)$:

$$E_i(F(\theta), \theta) = \int_0^{2\pi} \frac{j}{4} H_0^{(2)}(kr_0) J(\theta') d\theta'$$
$$+ j \sqrt{\frac{j}{\omega\mu_0\sigma(\theta)}} \frac{J(\theta)}{\sqrt{F^2(\theta) + F'^2(\theta)}}, \quad (4)$$

where

$$r_0(\theta, \theta') = [F^2(\theta) + F^2(\theta')$$
$$- 2F(\theta)F(\theta')\cos(\theta - \theta')]^{1/2}.$$

For the direct-scattering problem, the scattered field E_s is calculated by assuming that the shape and the conductivity of the object are known. This can be achieved by first solving J in eq. (4) and calculating E_s in eq. (2). For numerical calculation of the direct problem, the contour is first divided into sufficiently small segments such that the induced surface current density can be considered constant over each segment. Then the method of moments (MoM) [16] is used to solve eqs. (4) and (2) with a pulse-basis function for expanding and the Dirac delta function for testing.

Let us consider the following inverse problem: given the scattered field E_s, measured outside the scatterer, determine the shape $F(\theta)$ and conductivity $\sigma(\theta)$ of the object. Assume that the approximate center of the scatterer, which in fact can be any point inside the scatterer, is known. Hence, we can obtain the approximate position and the size of the cylinder by first using the tomography technique, and then obtain the exact solution by using our algorithm. Thus, the shape function $F(\theta)$ and conductivity function $\sigma(\theta)$ can be expanded as follows:

$$F(\theta) = \sum_{n=0}^{N/2} B_n\cos(n\theta) + \sum_{n=1}^{N/2} C_n\sin(n\theta), \quad (5)$$

$$\sigma(\theta) = \sum_{m=0}^{M/2} D_m\cos(m\theta) + \sum_{m=1}^{M/2} E_m\sin(m\theta), \quad (6)$$

where B_n, C_n, D_m, and E_m are real coefficients to be determined, and $(N + 1) + (M + 1)$ is the number of unknowns for the shape function and the conductivity function. Note that the discretization number $J(\theta)$ for the inverse problem must be different from that for the direct problem. Since it is crucial that the synthetic data be generated by a direct solver unlike those obtained by the inverse solver, the discretization number for the direct problem is two times that for the inverse problem in the simulation. In the inversion procedure, the genetic algorithm is used to minimize the following cost function:

$$\text{SF} = \left\{ \frac{1}{X_T} \sum_{x=1}^{X_t} \left| E_s^{\text{exp}}(\vec{r}_x) - E_s^{\text{cal}}(\vec{r}_x) \right|^2 / \sum_{x=1}^{X_t} \left| E_s^{\text{exp}}(\vec{r}_x) \right|^2 \right.$$
$$\left. + \beta[|F'(\theta)|^2] \right\}^{-1/2}, \quad (7)$$

where M_t is the total number of measured points, and $E_s^{\text{exp}}(\vec{r})$ and $E_s^{\text{cal}}(\vec{r})$ are the measured and calculated scattered fields, respectively. Note that the regularization term $\beta|F'(\theta)|^2$ was added in eq. (6). The minimization of $\beta|F'(\theta)|^2$ can, to a certain extent, be interpreted as the smoothness requirement for the boundary of $F(\theta)$. Therefore, the minimization of CF can be interpreted as the minimization of the least-squares error between the measured and calculated fields, with the constraint of a smooth boundary. Typical values of β range from 0.0001 to 10; but ideally, there is a decrease as convergence is attained [5]. The optimal value of β is mostly dependent on the dimensions of the geometry. One can always choose a large enough value to ensure the convergence, although overestimation will result in a very smooth reconstruction [5].

The genetic algorithms are global numerical-optimization methods based on genetic recombination and evolution in nature [13]. They use the iterative optimization procedures that start with a randomly selected population of potential solutions, and then gradually evolve toward a better solution through the application of the genetic operators: reproduction, crossover, and mutation. In our problem, all the parameters B_n, C_n, D_m, and E_m are given by the following equation:

$$B_n\ (C_n,\ D_m,\ \text{or}\ E_m) = p_{\min}$$
$$+ \frac{p_{\max} - p_{\min}}{2^L - 1} \sum_{i=0}^{L-1} b_i^{B_n\ (C_n, D_m,\ \text{or}\ E_m)} 2^i. \quad (8)$$
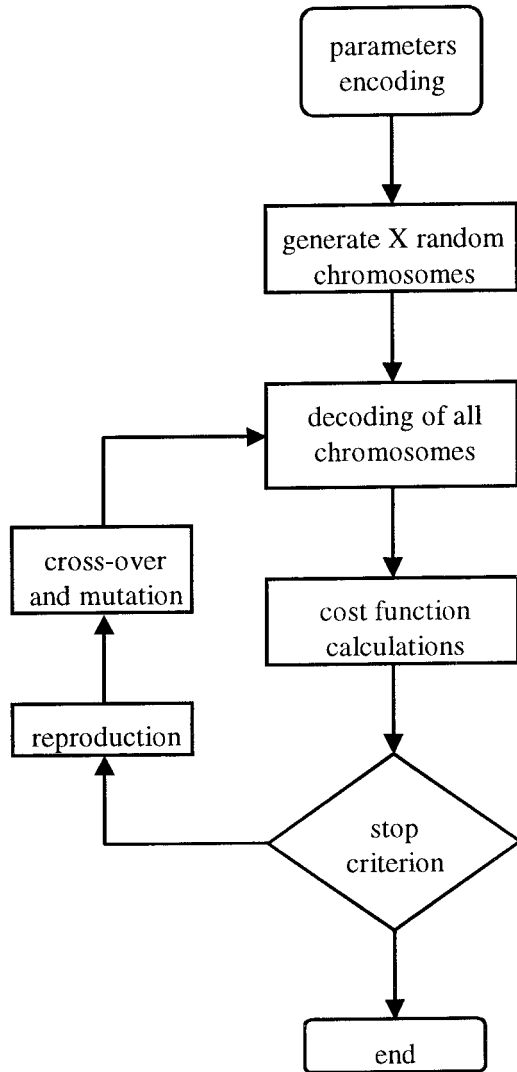
Figure 2. Flow chart for the genetic algorithm.

The $b_0^{B_n(C_n,D_m,\text{ or }E_m)}$, $b_1^{B_n(C_n,D_m,\text{ or }E_m)}$, ..., $b_{L-1}^{B_n(C_n,D_m,\text{ or }E_m)}$ (gene) is the L-bit string of the binary representation of B_n (C_n, D_m, or E_m), and p_{min} and p_{max} are the minimum and the maximum values admissible for B_n (C_n, D_m, or E_m), respectively. Here, p_{min} and p_{max} can be determined by prior knowledge of the object. Also, the finite resolution with which B_n (C_n, D_m, or E_m) can be tuned in practice is reflected in the number of bits assigned to it. The total unknown coefficients in eqs. (5), (6), and (8) would then be described by a $(M + N + 2) \times L$ bit string (chromosome). The basic GA, for which a flowchart is shown in Figure 2, starts with a large population that contains a total of X candidates. Each candidate is described by a chromosome. Then, the initial population can simply be created by taking X random chromosomes. Finally, the GA iteratively generates a new population, which is derived from the previous population through the application of the reproduction, crossover, and mutation operators.

The new populations will contain increasingly better chromosomes and will eventually converge to an optimal population that consists of the optimal chromosomes. As soon as the cost function (CF) changes by <1% in two successive generations, the algorithm will be terminated and a solution is thus obtained.

III. NUMERICAL RESULTS

By using a numerical simulation, we illustrate the performance of the proposed inversion algorithm and its sensitivity to random error in the scattered field. Let us consider an imperfectly conducting cylinder in free space and a plane wave of unit amplitude incident upon the object, as shown in Figure 1. The frequency of the incident wave is chosen to be 3 GHz; that is, the wavelength λ is 0.1 m. In the examples, the size of the scatterer is about one-third that of the wavelength, so the frequency is in the resonance range.

In our calculation, three examples are considered. To reconstruct the shape and conductivity of the cylinder, the object is illuminated by four incident waves with incident angles $\phi = 0°$, $90°$, $180°$, and $270°$, and the measurement is taken on a circle of radius R' at equal spacing. In our cases, R' is chosen to be much larger than $2D'^2/\lambda$, corresponding to the far-field measurement, where D' is the largest dimension of the scatterer. Note that for each incident angle, eight measurement points at equal spacing are used, and there are a total of 32 measurement points in each simulation. The number of unknowns is set to 14 ($M = 6$, $N = 6$) in order to save computing time. The population size is chosen as 300 (that is, $X = 300$). The binary string length of the unknown coefficient, B_n (C_n, D_n, or E_n), is set to be 16 bits (that is, $L = 16$). In other words, the bit number of a chromosome is 224 bits. The search range for the unknown coefficient of the shape function is chosen to be from 0 to 0.1 and the conductivity function is chosen to be from 10 to 100. The extreme value of the coefficient of the shape function and conductivity can be determined by prior knowledge of the objects. The crossover probability p_c and mutation probability p_m are set to be 0.8 and 0.2, respectively. The value of β is chosen to be 0.001.

In the first example, the shape and conductivity function are chosen to be $F(\theta) = (0.03 + 0.0025 \cos \theta - 0.005 \cos 2\theta + 0.005 \cos 3\theta)$ m and $\sigma(\theta) =$

$(80 + 12 \cos\theta + 10 \cos 2\theta + 8 \cos 3\theta + 12 \sin\theta + 15 \sin 2\theta + 18 \cos 3\theta)$ S/m. The reconstructed shape and conductivity function for the best population member (chromosome) are plotted in Figures 3(a) and
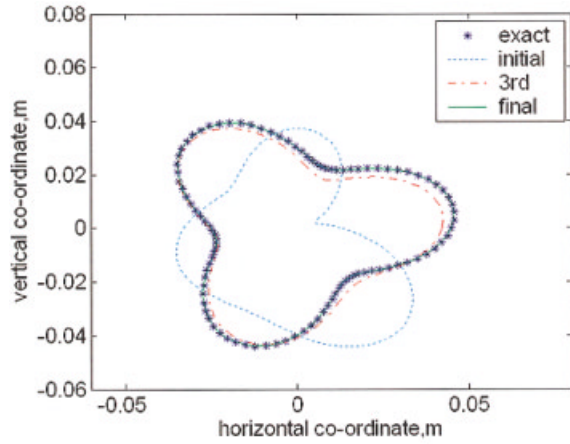
(a)
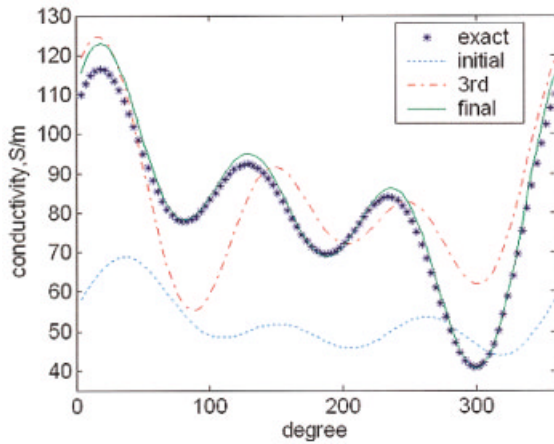
(b)
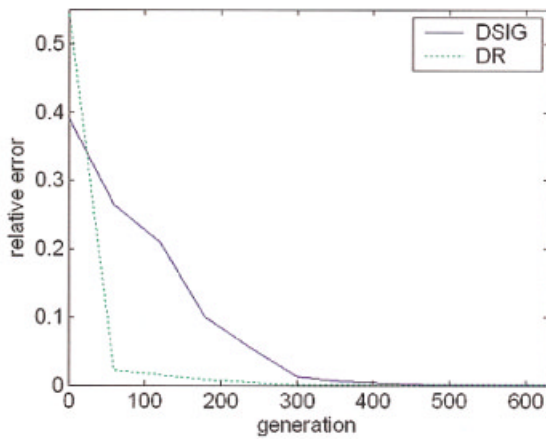
(c)
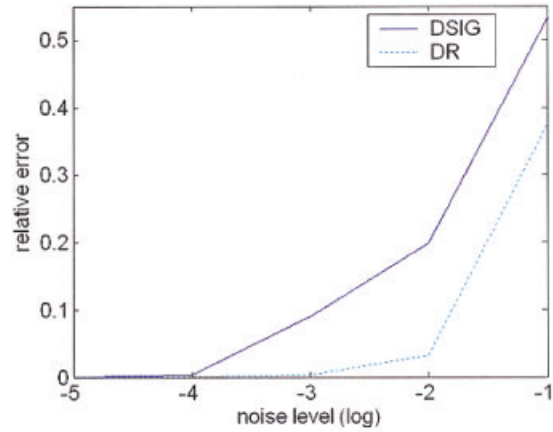
Figure 4. Relative error of shape and conductivity as a function of noise. [Color figure can be viewed in the online issue, which is available at www.interscience.wiley.com]

3(b); the error is shown in Figure 3(c), and the error for the reconstructed conductivity is also given in Figure 3(c). Here, DR and DSIG, which denote the shape-function and conductivity discrepancies, respectively, are defined as

$$\mathrm{DR} = \left\{ \frac{1}{N'} \sum_{i=1}^{N'} [F^{\mathrm{cal}}(\theta_i) - F(\theta_i)]^2 / F^2(\theta_i) \right\}^{1/2},$$

$$\mathrm{DSIG} = \left\{ \frac{1}{N'} \sum_{i'1}^{N'} [\sigma^{\mathrm{cal}}(\theta_i) - \sigma(\theta_i)]^2 / \sigma^2(\theta_i) \right\}^{1/2},$$

where N' is set to 60. The quantities DR and DSIG provide measures of how well $F^{\mathrm{cal}}(\theta)$ approximates $F(\theta)$ and $\sigma^{\mathrm{cal}}(\theta)$ approximates $\sigma(\theta)$, respectively. From Figures 3(a) and 3(b), it is clear that the reconstruction of the shape and the conductivity function is quite good. In addition, we also see that the reconstruction of conductivity does not change rapidly toward the exact value until DR is small enough. This can be explained by the fact that the shape function makes a stronger contribution to the scattered field than the conductivity does. In other words, the recon-

Figure 3. (a) Shape function for example 1: the star curve represents the exact shape, while the solid curves are calculated shape in iteration process; (b) conductivity function for example 1: the star curve represents the exact conductivities, while the solid curves are the calculated conductivities in the iteration process; (c) shape and conductivity function error in each generation. [Color figure can be viewed in the online issue, which is available at www.interscience.wiley.com]

struction of the shape function has a higher priority than the reconstruction of the conductivity. To investigate the sensitivity of the imaging algorithm against random noise, two independent Gaussian noises with zero mean have been added to the real and imaginary parts of the simulated scattered fields. Normalized standard deviations of 10^{-5}, 10^{-4}, 10^{-3}, 10^{-2}, and 10^{-1} are used in the simulations. The normalized standard deviation mentioned previously is defined as the standard deviation of the Gaussian noise divided by the rms value of the scattered fields. Here, the signal-to-noise ratio (SNR) is inversely proportional to the normalized standard deviation. The numerical result for this example is plotted in Figure 4. It is


(a)

(a)

(b)
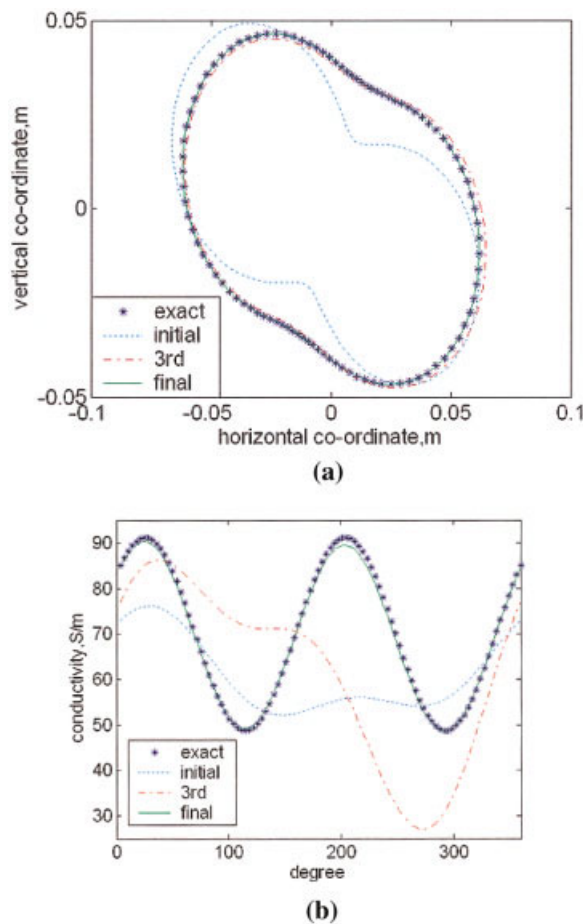
Figure 5. (a) Shape function for example 2: the star curve represents the exact shape, while the solid curves are the calculated shape in the iteration process; (b) conductivity function for example 2: the star curve represents the exact conductivity, while the solid curves are the calculated conductivities in the iteration process. [Color figure can be viewed in the online issue, which is available at www. interscience.wiley.com]

(b)
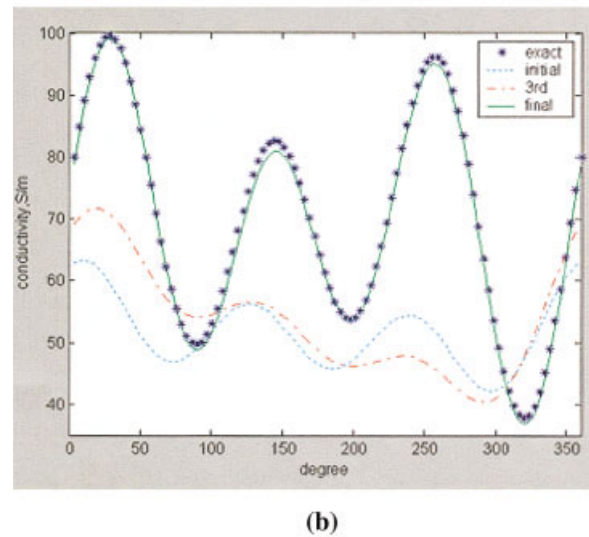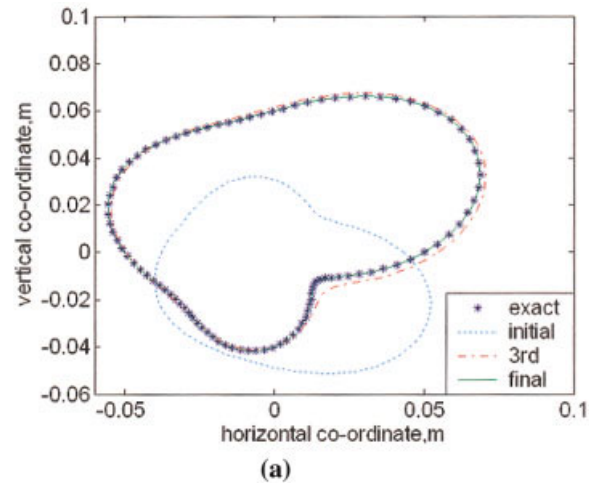
Figure 6. (a) Shape function for example 3: the star curve represents the exact shape, while the solid curves are the calculated shape in the iteration process; (b) conductivity function for example 3: the star curve represents the exact conductivity, while the solid curves are the calculated conductivities in the iteration process. [Color figure can be viewed in the online issue, which is available at www. interscience.wiley.com]

understood that the effect of noise is negligible for normalized standard deviations below 10^{-3}.

In the second example, we selected a peanut shape $F(\theta) = (0.05 + 0.01 \cos 2\theta - 0.01 \sin 2\theta)$ m and a conductivity function $\sigma(\theta) = (70 + 15 \cos 2\theta + 15 \sin 2\theta)$ S/m. The purpose of this example is to show that our method is able to reconstruct different shapes of conductivity. Satisfactory results are shown in Figures 5(a) and 5(b).

In the third example, the shape and the conductivity function are selected to be $F(\theta) = (0.05 + 0.02$

$\sin \theta + 0.01 \sin 2\theta + 0.01 \sin 3\theta$) m and $\sigma(\theta) =$ (70 + 10 $\cos 3\theta$ + 10 $\sin 2\theta$ + 20 $\sin 3\theta$) S/m, respectively. Note that the shape function is not symmetrical with regard to either the x axis or the y axis. This example further verifies the reliability of our algorithm, as shown in Figures 6(a) and 6(b) in detail.

IV. CONCLUSION

We have presented a study of applying the genetic algorithm to reconstruct the shape and conductivity of a metallic object through knowledge of the scattered field. Based on the boundary condition and measured scattered field, we have derived a set of nonlinear integral equations and reformulated the imaging problem into an optimization problem. By using the genetic algorithm, the shape and conductivity of the object can be reconstructed. Even when the initial guess is far from exact, the genetic algorithm converges to a global extreme of the cost function, whereas gradient-based methods often get stuck in a local extreme. Good reconstruction has been obtained from the scattered fields both with and without the additive Gaussian noise. Numerical results also illustrate that the conductivity is more sensitive to noise than the shape function. According to our experience, the main difficulties in applying the genetic algorithm to this problem are how to choose the parameters, such as the population size M, bit length of the string L, crossover probability p_c, and mutation probability p_m. Different parameter sets will affect the speed of convergence, as well as the computing time required. From the numerical simulation, it is concluded that a population size from 300 to 600, a string length from 8 to 16 bits, and p_c and p_m in the ranges of $0.7 < p_c < 0.9$ and $0.0005 < p_m < 0.05$, respectively, are suitable for imaging problems of this type.

ACKNOWLEDGMENT

REFERENCES

1. T. Hohage, Iterative methods in inverse obstacle scattering: Regularization theory of linear and nonlinear exponentially ill-posed problems, Dissertation Linz, 1999.

2. C.C. Chiu and Y.W. Kiang, Electromagnetic imaging for an imperfectly conducting cylinders, IEEE Trans Microwave Theory Tech 39 (1991), 1632–1639.

3. R. Kress, A Newton method in inverse obstacle scattering Inverse Problem in Engineering Mechanics, H.D. Bui et al. (Eds.). Balkema, Rotterdam, 1994, pp. 425–432.

4. C. Chat-Uthai, J.A. Ramirez, and E.M. Freeman, An improved constrained quasi-Newton method for the solution of inverse electromagnetic problems, IEEE Trans Magnetics 32 (1996), 1318–1321.

5. G.P. Otto and W.C. Chew, Microwave inverse scattering, local shape-function imaging for improved resolution of strong scatterers, IEEE Trans Microwave Theory Tech 42 (1994), 137–141.

6. D. Colton and P. Monk, A novel method for solving the inverse scattering problem for time-harmonic acoustic waves in the resonance region II, SIAM J Appl Math 46 (1986), 506–523.

7. A. Kirsch, R. Kress, P. Monk, and A. Zinn, Two methods for solving the inverse acoustic scattering problem, Inverse Problems 4 (1988), 749–770.

8. F. Hettlich, Two methods for solving an inverse conductive scattering problem, Inverse Problems 10 (1994), 375–385.

9. R.E. Kleinman and P.M. van den Berg, Two-dimensional location and shape reconstruction, Radio Sci 29 (1994), 1157–1169.

10. C.C. Chiu and P.T. Liu, Image reconstruction of a perfectly conducting cylinder by the genetic algorithm, IEE Proc Microwave Antennas Propagat 143 (1996), 249–253.

11. Z.Q. Meng, T. Takenaka, and T. Tanaka, Image reconstruction of two-dimensional impenetrable objects using genetic algorithm, J Electromagn Waves Applic 13 (1999), 95–118.

12. Z. Qian, Z. Ding, and W. Hong, Application of genetic algorithm and boundary element method to electromagnetic imaging of two-dimensional conducting targets, Proc 5th Int Symp Antennas Propagat EM Theory (2000), 211–214.

13. D.E. Goldgerg, Genetic algorithm in search, optimization and machine learning, Addison-Wesley, 1989.

14. F.M. Tesche, On the inclusion of loss in time domain solutions of electromagnetic interaction problems, IEEE Trans Electromagn Compat 32 (1990), 1–4.

15. E.C. Jordan and K.G. Balmain, Electromagnetic waves and radiating systems, Prentice-Hall, Englewood Cliffs, NJ, 1968.

16. R.F. Harrington, Field computation by moment methods, Macmillan, New York, 1968.

BIOGRAPHIES
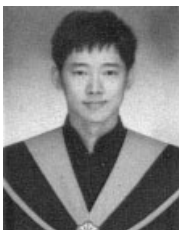
Wei Chien was born in Taipei, Taiwan, Republic of China, on April 21, 1974. He received his B.S.E.E. degree from Tatung Institute of Technology, Taipei, Taiwan, in 1997 and his M.S.E.E. degree from Tamkang University, Taipei, Taiwan, in 1999. From 1999 to 2001, he served in the ROC Army Force as a second lieutenant. He is currently working toward Ph.D. degrees in the Department of Electrical Engineering, Tamkang University. His current research interests include numerical techniques in electromagnetics and wireless communications.

Chien-Ching Chiu was born in Taoyuan, Taiwan, Republic of China, on January 23, 1963. He received his B.S.C.E. degree from National Chiao Tung University, Hsinchu, Taiwan, in 1985 and M.S.E.E. and Ph.D. degrees from National Taiwan University, Taipei, Taiwan, in 1987 and 1991, respectively. From 1987 to 1989, he served in the ROC Army Force as a communication officer. In 1992 he joined the faculty of the Department of Electrical Engineering, Tamkang University, where he is now a Professor. He was a visiting scholar at MIT and University of Illinois, Urbana, from 1998 to 1999. His current research interests include microwave imaging, numerical techniques in electromagnetics, and indoor wireless communications.